Sensors & Actuators: B. Chemical 370 (2022) 132421

Contents lists available at ScienceDirect

Sensors and Actuators: B. Chemical

journal homepage: www.elsevier.com/locate/snb

Smartphone enabled upconversion nanoparticle-based lateral flow strip for ultra-low concentration of methamphetamine detection

Wei Wang [b], Zihan Ye [c], Xing Ma [c,*], Jinhong Guo [a,b,**]

[a] School of Sensing Science and Engineering, Shanghai Jiao Tong University, Shanghai 200240, China
[b] School of Information and Communication Engineering, University of Electronic Science and Technology of China, Chengdu 611731, China
[c] School of Materials Science and Engineering, Harbin Institute of Technology (Shenzhen), Shenzhen 518055, China

ARTICLE INFO

Keywords:
Methamphetamine testing
Lateral flow assays
Upconversion nanomaterials
Point-of-care testing
Internet of medical things
Computer vision

ABSTRACT

The combination of upconversion nanoparticles (UCNPs) and Lateral Flow Assays (LFAs) is becoming one of the most desirable quantitative assays for point-of-care testing (POCT) due to their excellent chemical and optical properties, which make them commercially viable as fast, sensitive and portable. We propose upconversion nanoparticle-based lateral flow assays (UCNP-LFAs) combined with computer vision for the instantaneous detection of small molecule targets in a commercial medical device. The device overcomes the traditional lengthy pre-processing and ambiguous qualitative results, where computer vision algorithms improve the sensitivity and robustness of quantitative results. Compared with the standard quantitative testing process, the accuracy of its quantitative test results was improved by 17.4%. The device detected and reported the quantitative results of Methamphetamine (MET) concentration with the lower limit of detection (LOD) of 0.1 ng/ml in 20 s in field tests. Its success demonstrated good sensitivity, repeatability, and robustness. Most importantly, the entire device measures only 100 mm * 120 mm* 74 mm and weighs 351.2 g, combining portability and immediacy and providing quantitative data for small molecule targets at a lower concentration. This makes our system an extraordinarily creative and attractive approach, especially for applications in complex field environments with chaotic personnel and special emergencies.

1. Introduction

POCT is a new field in laboratory medicine development and one of the most promising fields in the In-Vitro Diagnostics (IVD) industry [1–5]. LFAs are the most advantageous form of diagnostic field testing [6–8]. Due to their potential for miniaturization, simplicity of operation, and immediate reporting of results, LFAs are widely used for immediate testing in-home and roadside field testing scenarios. They are inexpensive and straightforward to use, especially in countries and regions with relatively low medical standards. The many advantages of immunochromatographic test strips make them an Affordable, Sensitive, Specific, User-friendly, Rapid/Robust, Equipment-free, and Deliverable (ASSURED) technology for POCT. To realize and meet the growing demand for rapid on-site quantitative testing, researchers are constantly striving to find new strategies to develop POCT devices with greater accuracy, sensitivity, robustness, immediacy, ease of use, and quantitative analysis on a portable scale. In recent years, high-tech companies and researchers have continued to improve various existing devices and instruments to achieve a range of results [9–12], especially concerning IoT solutions for POCT scenarios built based on smartphones with their near-ubiquitous distribution. LFAs technology and smartphones can communicate in the field inspection environment through communication technology such as 5 G or Bluetooth. Due to the prevalence of smartphones and the high performance of modern cell phone processors, coupled with the low cost of LFAs technology, real-time quantitative detection platforms for POCT scenarios will be an essential trend in the future and introduce a “technological revolution” in the field of POCT.

Upconversion Luminescence (UCL) is a luminescence phenomenon in which rare earth ions absorb two or more low-energy photons and radiate high-energy photons and is a form of anti-Stokes luminescence [13–15]. With the emergence of nanotechnology, UCL has been used as an infrared to visible light conversion material in many fields such as biomedicine, drug detection, and food safety. Compared with traditional organic dyes and semiconductor quantum dots such as down-conversion

* Corresponding author.
** Corresponding author at: School of Sensing Science and Engineering, Shanghai Jiao Tong University, Shanghai 200240, China.
E-mail addresses: maxing@hit.edu.cn (X. Ma), guojinhong@sjtu.edu.cn (J. Guo).

https://doi.org/10.1016/j.snb.2022.132421
Received 5 January 2022; Received in revised form 22 June 2022; Accepted 23 July 2022
Available online 30 July 2022

luminescent materials, UCNPs, as a new generation of fluorescent markers, have a series of significant advantages such as high chemical stability, outstanding emission spectral features, use of near-infrared as the excitation source, long fluorescence lifetime and high detection sensitivity [16–18].

By measuring the fluorescence intensity on Test Line (TL) and Control Line (CL) on UCNPs-based Lateral Flow Strips, quantitative detection was achieved by calculating the CL and TL ratio [19–23]. Hu et al. proposed the use of UCNPs for drug detection by using morphine (MOP) and MET in saliva as target molecules and obtaining accurate quantitative results by calculating the fluorescence intensity ratio of CL and TL on test strips, which demonstrated that UCNPs-based Lateral Flow Strips could be applied to roadside detection of drug abuse [24]. Mei et al. obtained UCNPs-based paper sensors capable of rapid, sensitive, and quantitative detection of the pesticide thiram in apple juice by immersing them in $NaYF_4:Yb/Tm$ upconversion nanoprobes [25]. Zhao et al. constructed a UCNPs-based luminescence detection instrument for the rapid quantitative detection of MOP. They obtained more accurate quantitative results using the instrument's fluorescence intensity ratio of TL/CL and an excellent linear correlation by fitting a standard solution containing MOP [26]. Rohit et al. report a UCNP-based signal enhancement strategy for the detection of tetrahydrocannabinol. By adding an additional enhancement pad (EP), the clustering of the target detectors on the test line was achieved, which resulted in a 20% increase in the displayed test intensity. The signal enhancement strategy proved important for improving sensitivity and accuracy of the test results [27]. Moreover, these UCNP-LFAs based detection devices are gradually moving toward portability, such as Jung et al. accurately detecting food-borne bacteria E. coli by a smartphone-based lateral flow imaging system [28], and Xiao et al. designed a small smartphone-based quantitative colloidal gold lateral flow immunoassay strip readout device [29]. Jin et al. proposed a device that can detect multiple target detectors simultaneously by combining UCNP-LFAs with a smartphone [30]. Min et al. designed a smartphone-based lateral flow analyzer for rapid quantitative detection of Salmonella spp. Using machine learning-enhanced algorithms [31]. Kim et al. report an integrated bioluminescence readout system consisting of a sample holder with associated enhanced algorithms that effectively translate luminescence intensity to concentration for a bacterial sample [32]. In addition, many commercial companies are developing more compact-based rapid testing equipment[30]. Labrox and Hidex of Finland have recently investigated a digital display readout device for upconversion fluorescent probes[33,34]. However, to our knowledge, there is a lack of commercially available devices that detect upconverted fluorescent nanomaterials.

As a global social problem, the proliferation of drugs has become a significant influence on human health and a threat to social stability. In recent years, the global production of MET has increased significantly, and how to make an effective, rapid, accurate, and stable determination of MET and other drugs has become an urgent problem. There have been several ways to detect MET, High-Performance Liquid Chromatography (HPLC) [35,36], Gas Chromatography-Mass Spectrometry (GC-MS) [37,38], Liquid Chromatograph-Mass Spectrometer (LC-MS) [39], Capillary Electrophoresis (CE) [40,41], Fluorescent Detection (FD) [24,42,43], Surface Plasmon Resonance (SPR) [44], etc. [45–48] However, these methods have different degrees of cross-reactivity, many interfering factors, a complex pretreatment process, the low LOD, a long detection time, and instrumentation. However, all these methods have different degrees of cross-reactivity, many interfering factors, complicated pre-processing, the low LOD, long detection time, and expensive and bulky instruments. Most importantly, most MET and other drug testing cards can only qualitatively detect the presence of drugs, but not quantitatively or semi-quantitatively. These disadvantages greatly limit MET and other drugs' quantitative and immediate detection.

Based on the above background study, we introduce UCNPs into LFAs and obtain quantitative detection results of target molecules by analyzing the fluorescence signal from fluorescent nanomaterials (Fig. 1). Specifically,

- A portable and ultra-sensitive upconversion fluorescent probe-based commercial-type biosensor for in situ detection was designed.
- A computer vision-based image denoising model was constructed to apply it to fluorescence intensity extraction, significantly improving specificity and sensitivity.
- A waveform reconstruction method based on the Gaussian function is proposed, and the sensitivity and robustness of the quantitative detection results of the target test substance are greatly improved by this innovative signal processing method.
- A complete and pervasive Internet of Things (IoT) solution based on UCNPs detection is established.

Finally, through a series of standard and actual field tests, we use MET as the quantitative test target to verify the device's effectiveness and obtain satisfactory results. The experimental analysis of the quantitative test shows that the system has high accuracy and repeatability, with instant and quantitative detection in the field environment.

2. Materials and methods

2.1. Chemicals and materials

The oleic acid (OA), 1-octadecene (ODE), yttrium (III) chloride ($YCl_3 \bullet 6H_2O$), ytterbium chloride($YbCl_3 \bullet 6H_2O$), erbium chloride ($ErCl_3 \bullet 6H_2O$), cyclohexane, cetyltrimethylammonium bromide (CTAB), methanol, ethanol (EtOH), N, N-Dimethylformamide (DMF), succinic anhydride (SAA), triethylamine (TEA), and 1-ethyl-3-(3-dimethyl aminopropyl)-carbodiimide (EDC) was purchased from Shanghai Macklin Biochemical Technology Co., Ltd (China). The tetraethyl orthosilicate (TEOS), (3-aminopropyl)triethoxysilane (APTES), N-hydroxysuccinimide (NHS), bovine serum albumin (BSA), 2-(N-morpho-line)-ethane sulphonic acid (MES, ultra-pure grade, 99.0%), T-casein, Tris, polyvinyl pyrrolidone (PVP), Sodium hydroxide (NaOH) and ammonium fluoride (NH_4F) were purchased from Sigma-Aldrich (Shanghai, China). MET monoclonal antibodies (MET-MAbs) and MET antigens were obtained from CUSABIO (Wuhan, China). The goat anti-mouse IgG was obtained from Artron BioResearch Inc (Shandong, China). Milli-Q-purified water of 18.2 $M\Omega$ at 25℃ was used throughout the experiment.

2.2. Synthesis of $UCNPs@SiO_2$

Based on our previous results [49], the preparation was divided into three steps. In the first step, the typical synthesis of $NH_4F:Yb,Er$ (Yb:20 mol, Er^{3+}:2 mol%), $YCl_3 \bullet 6H_2O$ (1.56 mmol), $YbCl_3 \bullet 6H_2O$ (0.40 mmol) and $ErCl_3 \bullet 6H_2O$ (0.04 mmol) was performed. and $ErCl_3 \bullet 6H_2O$ (0.04 mmol) was initially needed, and the rest of the experimental procedure was based on the literature [50]. In the second step, encapsulate *UCNPs* with SiO_2 Which is according to literature protocols [51]. In the third step, Carboxyl functionalization of $UCNPs@SiO_2$. The prepared $UCNPs@SiO_2$ (50 mg) was initially dispersed in 10 ml *EtOH*. 100μL APTES was then added into the solution and stirred for 24 h. The resulting product $UCNPs@SiO_2-NH_2$ was collected by centrifugation and washing (3 times with *EtOH*). Subsequently, the prepared $UCNPs@SiO_2$ was dispersed in 10 ml of *DMF*. 50 mg of SAA and 52.1μL of TEA were then added into the solution and stirred for another 24 h. After three times of centrifugation and washing (with *EtOH* and *DMF*), the resulting products $UCNPs@SiO_2-COOH$ was finally obtained, which were used as luminescent labels in LFAs for MET quantification. Specifically, the characterization of the UCNPs probes is shown in Figs. 2a-2f.

Fig. 1. Design a portable, commercial device for rapid quantitative drug testing in the field and its accompanying mobile data analysis application.

2.3. Preparation of UCNP-LFAs

The Lateral Flow Assay sensor consists of a sample pad, a binding pad, a nitrocellulose (NC) membrane, an absorbent filter paper combined and mounted on a base card. The sample pad is used for dripping the sample solution to be tested; the binding pad is used for pre-spraying the up-converted fluorescent detection probes prepared; the NC membrane is used for pre-fixing the capture and control probes to form the TL and CL, respectively; and the absorbent filter paper provides capillary force and prevents reflux of the sample solution. The Lateral Flow Assay sensor is fabricated by using a three-dimensional scribe to spray the upconversion fluorescence detection probe on the binding uniformly, and the capture probe and control probe on the NC membrane to form TL and CL, respectively, and then the pretreated binding pad and NC membrane are dried in an oven. After drying, the binding pad and NC film are assembled on the backing card, and the backing card is cut with a chopper. A unique QR code (which contains all relevant information about the test strip) is printed on the top end of each sensor to facilitate access to the information of the test strip (target detectors, expiration date, generation batch, etc.) via IoT devices/PC scanning to obtain the final Lateral Flow Assay sensor. Because MET has a low molecular weight and a single antigenic determinant cluster, the Lateral Flow Assay sensor is based on antigen-antibody binding and uses a competition method (Fig. 2g).

2.4. Design of hardware and mobile application software for UCNP-LFAs-based fluorescence detector

The hardware structure of the upconversion fluorescence quantification detection sensor is shown in Fig. 3a, and the real internal composition of the device is shown in Fig. 3b. Moreover, Fig. 3c shows the design appearance of the final device. The above diagrams show that the device comprises a 980 nm laser, a custom guide, a filter, a CMOS camera, a stepper motor, a microcontroller unit, a Bluetooth data transmission unit, and a USB/Bluetooth interface.

The smartphone-based quantitative analysis application that we built is shown in Fig. 3e. To make it easier for relevant law enforcement officers to conduct on-site drug detection and long-term tracking and investigation of drug users, we provide a complete drug detection and anti-drug situational awareness system. (1) Through information registration and the generation of QR codes, including personal information of detectors, test results, and other valid information (e.g., drug type detected, time of detection, location of detection, etc.). The information is also stored in the police department's database for situational drug awareness in a standardized manner according to individual codes. (2) Control the detection instrument to start and set the detection conditions. For example, the type of drugs detected, the number of repetitions, etc. Finally, automatic analysis of image data is performed, and detection reports are automatically generated. (3) A big database analysis and management system with multiple functions. For example, the addition, deletion, change, query, and export of data. Most importantly, an anti-drug situational awareness system can be constructed based on this rich data.

2.5. Workflow of quantitative detection using UCNP-LFAs based fluorescence detector

In the upconversion luminescence system, the QR code on the Lateral Flow Assay sensor is first scanned using the accompanying cell phone application to obtain the information stored in the QR code. After inserting the lateral flow assay sensor into the custom guide, the upconversion luminescence detector is started on the cell phone application. The MCU controls the stepper motor to drag the Lateral Flow Assay sensor at a constant speed and direction. In addition, a series of amplifiers, cameras, and other controls cooperate to acquire the video image stream signal. The Lateral Flow Assay sensor then transmits the acquired image data to the cell phone via Bluetooth; finally, the cell phone receives the image data and processes it to automatically generate the results displayed on the cell phone screen (Fig. 4).

It is worth stating that to enhance the accuracy and robustness of the device in collecting raw image data. Through a clever special design, the detection of two insertions at once is achieved. When the LFAs are inserted into the stepper motor, the detection process is mainly divided into two phases, "Push" and "Pull", and the signals are symmetrically distributed in the time series. Therefore, each data set in the data image processing stage is the average of these two original data points(Fig. 3f). This clever design does not add additional detection time, and it was confirmed in the validation phase that the design dramatically improves the robustness of the device.

3. Computer vision-based signal enhancement algorithm

In previous studies, researchers focused more on hardware design and development but lacked adequate attention to the image processing of the fluorescent images captured by the camera. The research in this paper found that practical image processing algorithms can improve the final quantitative detection results by about 16%. While the upconversion fluorescent material solves the problem of auto-fluorescence interference by eliminating background interference from endogenous fluorescent substances and simultaneously labelled fluorescent dyes, the detection background value is reduced, and the detection sensitivity is improved. However, unlike large laboratory equipment with a stable experimental environment, this equipment is suitable for immediately detecting a complex operating environment, subject to many

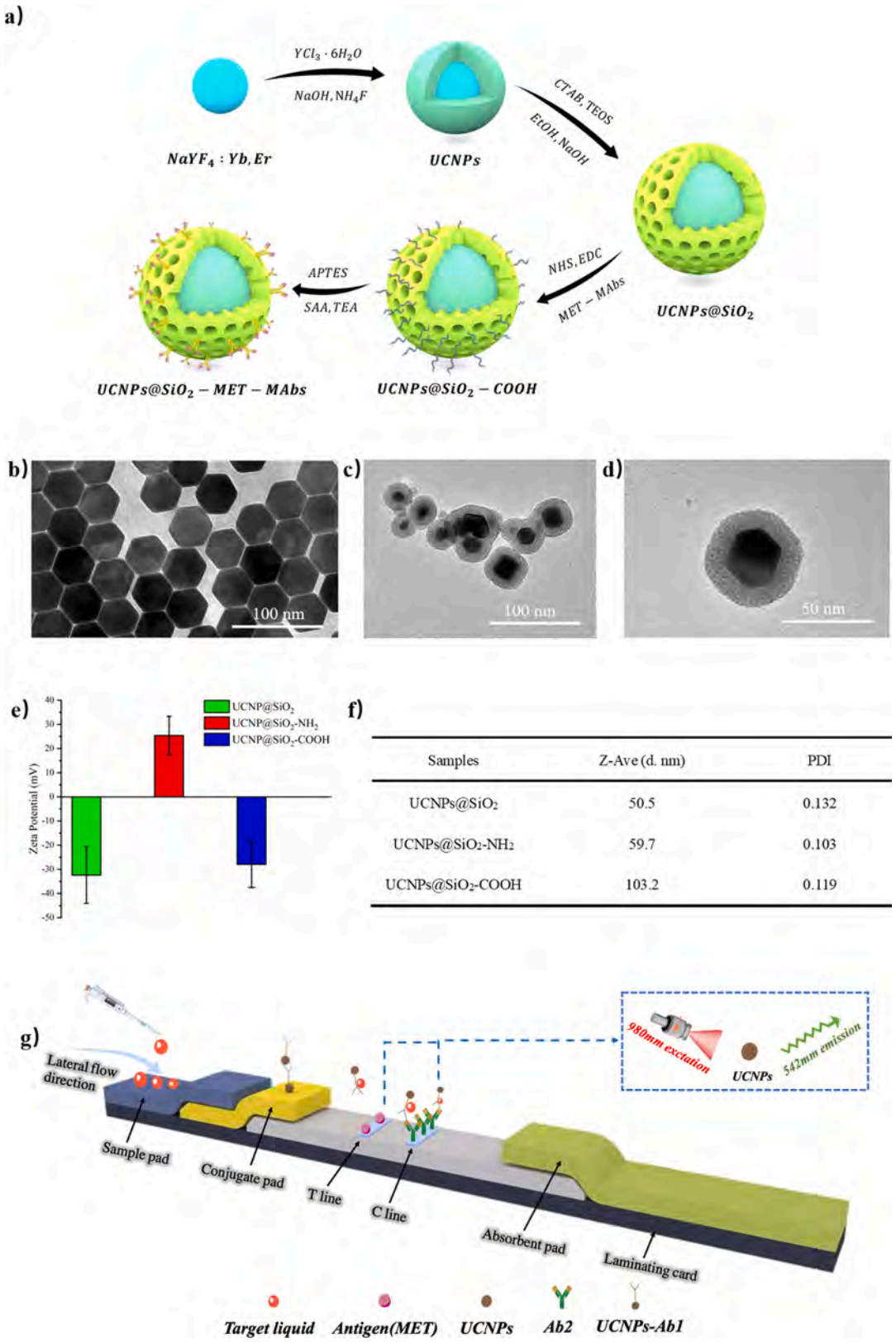

Samples	Z-Ave (d. nm)	PDI
$UCNPs@SiO_2$	50.5	0.132
$UCNPs@SiO_2$-NH_2	59.7	0.103
$UCNPs@SiO_2$-COOH	103.2	0.119

Fig. 2. (a) Schematic diagram of the preparation of UCNPs) detection probes. TEM images of b) UCNPs, c) *UCNPs@SiO*$_2$ and d) Enlarged *UCNPs@SiO*$_2$. The prepared UCNPs have a hexagonal phase structure with homogeneous size and no aggregation, indicating that the prepared UCNPs have good dispersibility. (e) Zeta potential characterization plots of *@SiO*$_2$, *UCNPs@SiO*$_2$ $-NH_2$ and *UCNPs@SiO*$_2$ – COOH. The change process of zeta potential in the figure confirms the successful modification of the corresponding functional group. (f) The particle size distribution of *UCNPs@SiO*$_2$, *UCNPs@SiO*$_2$ $-NH_2$ and *UCNPs@SiO*$_2$ – COOH. (g) Schematic diagram of UCNP-LFAs.

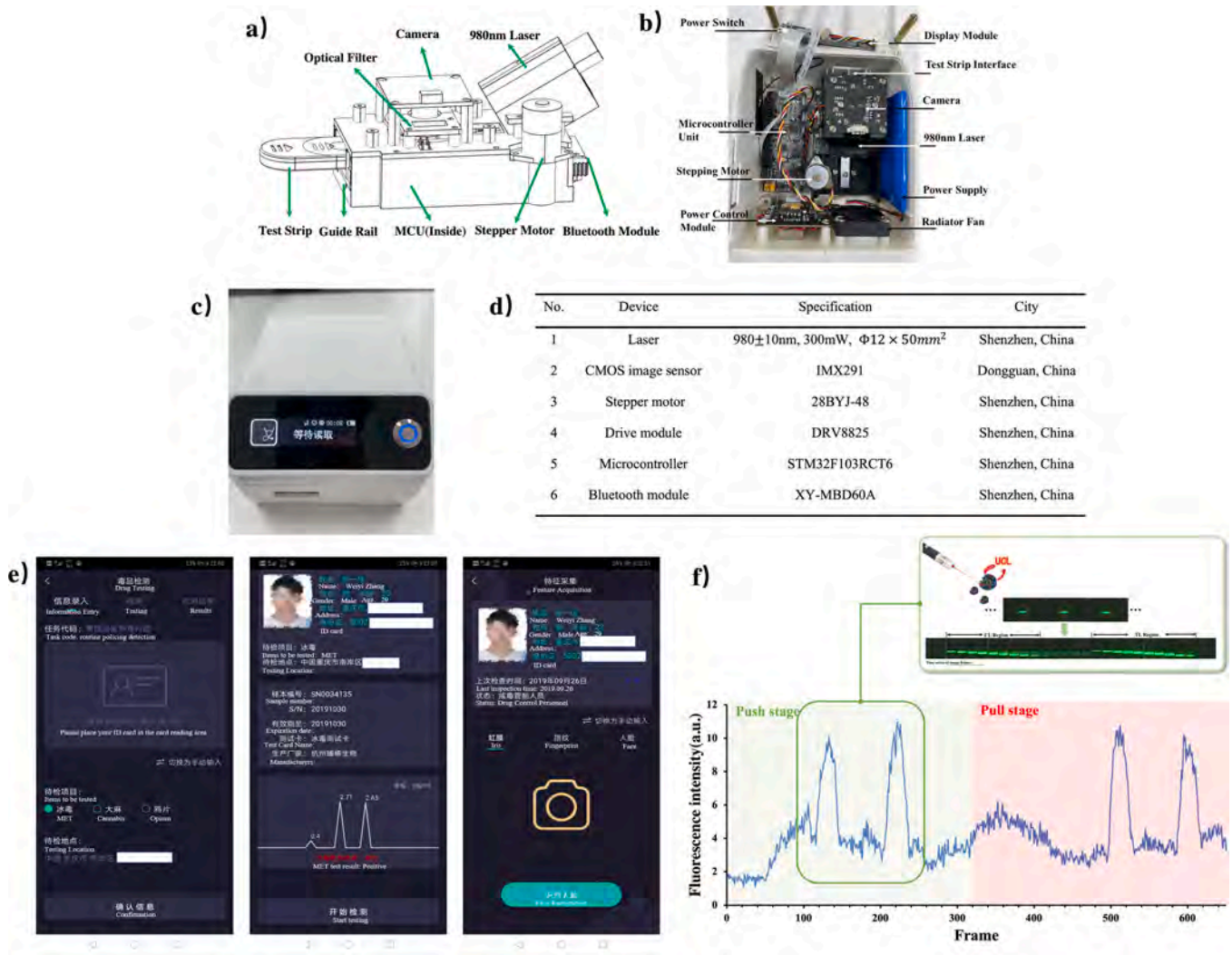

No.	Device	Specification	City
1	Laser	980±10nm, 300mW, $\Phi 12 \times 50mm^2$	Shenzhen, China
2	CMOS image sensor	IMX291	Dongguan, China
3	Stepper motor	28BYJ-48	Shenzhen, China
4	Drive module	DRV8825	Shenzhen, China
5	Microcontroller	STM32F103RCT6	Shenzhen, China
6	Bluetooth module	XY-MBD60A	Shenzhen, China

Fig. 3. (a) Hardware structure diagram of the device. (b) Diagram of the real internal composition of the device. The device has a simple and compact internal design and can be used directly for commercial purposes. The device is a combination of portability, high sensitivity and low-cost quantitative detection biosensor based on UCNPs. (d)The main component of the upconversion luminescence biosensor. (e) Smartphone-based quantitative analysis application. It is mainly used for test result display, medical health data storage and analysis, and also provides data support for future disease prevention. (f)The detection device captures the original fluorescence intensity signal at a concentration of 10 ng/ml. From the start of the stepper motor movement to the end, the image sensor continuously captures the image of the specified area and outputs the fluorescence intensity. Due to the special design of the device, it is possible to insert the test twice at once. It can be seen that the detection process is mainly divided into two phases, "Push" and "Pull", and the signal is symmetrically distributed in the time series. The final quantitative detection is obtained by averaging the results of the two phases, which further enhances the stability of the device in the field environment. This design further enhances the stability of the device in the on-site environment.

environmental factors and hardware interference factors (Figs. 5a and 5b). Therefore, the removal of background noise interference improves the accuracy of the results significantly.

The device obtained the quantitative results of the target material by calculating the fluorescence intensity ratio of CL/TL; thus, the fluorescence intensity information of CL and TL on the test strips is used as a vital data indicator for the quantitative detection of MET. First, the stepper motor always drags the Lateral Flow Assay sensor at a constant speed and direction because the 980 nm laser and camera position posture is fixed in the hardware design module. It is easy to conclude that the fluorescence excitation area will be limited to a small position. Second, the fluorescence excitation appearance time will be limited to a short time. In other words, we can limit the image processing to a fixed rectangular area in the camera capture image without the need for an additional fluorescence area localization algorithm. Therefore, the whole algorithm focuses on the denoising and enhancement of the obtained video stream signal. Third, the obtained fluorescence intensity signal can be approximated as a Gaussian curve on the time series.

In the image pre-processing stage, the specific steps are as follows: (1) the region of interest (ROI) is selected in a fixed rectangular area of the capture screen; (2) as the fluorescence emits green light, only the green channel is selected after separating the three channels of the image RGB, thus obtaining a green single-channel image; and (3) Gaussian low-pass filtering is performed on the image to eliminate high-frequency noise interference. More ablation experiments will be shown in the Results and Discussion to verify the effectiveness of the two algorithms proposed below.

3.1. Image adaptive binarization

The previous study performed extensive work on the captured video stream signal to study the image background noise distribution. Fig. 5a shows the image histograms of three representative image frames. An image histogram is a statistical table that reflects the distribution of image pixels. The horizontal coordinate represents the grayscale of the image pixels, and the vertical coordinate represents the total number of

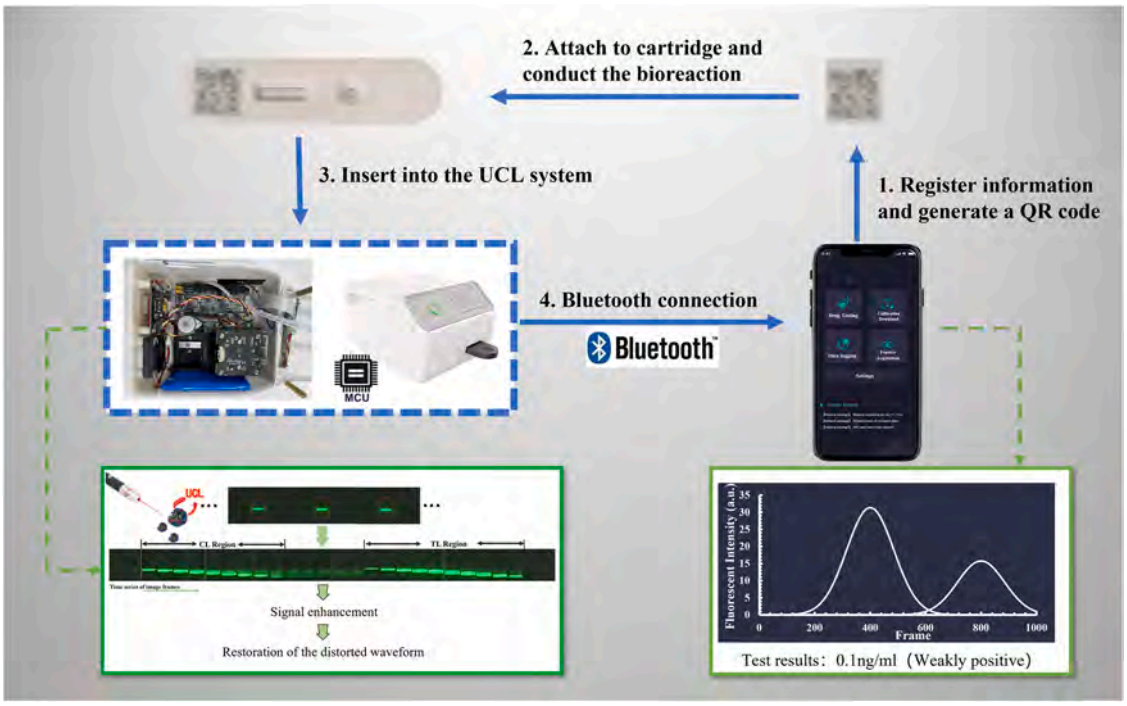

Fig. 4. UCNPs-based lateral flow assay operation flow. First, the inspector/enforcement officer collects information about the testers and generates a unique QR code to be pasted on the unused LFAs, then, the LFAs are inserted into the test device's filling hole and the device runs the analysis automatically by pressing the "Start" button. The results will be displayed on the device display or transferred to a smartphone via Bluetooth. As shown in the figure, the actual on-site test usually requires only 0.2 ng/ml LOD, so the device displays the quantitative results with the label "Weakly positive".

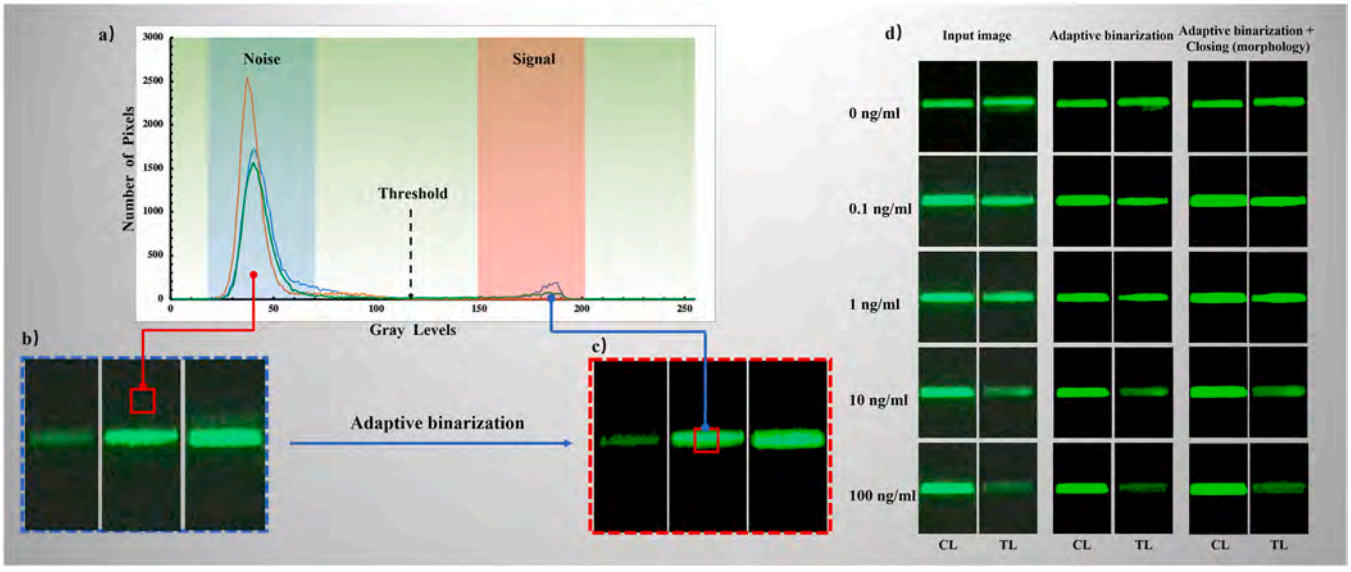

Fig. 5. Comparison of image pixel statistical distribution and denoising algorithm processing based on fluorescent video streams. (a) Grayscale histogram of the original image without denoising. All pixels in the captured fluorescent image are counted according to their frequency of occurrence in terms of the magnitude of grayscale values. (b) The original image without denoising. (c) Fluorescence image after adaptive binarization process. (d) The sequence of original images with different concentrations after adaptive binarization and the closing (morphology).

pixels in the image for each grayscale value. Because an image is composed of pixels, the histogram reflecting the pixel distribution is an essential feature of an image. Fig. 5a shows that the pixel distribution has a "bimodal" shape. The blue area on the left gathers many low grayscale values piled up into a crest, mainly formed by stray light and thermal noise and other environmental factors causing low-frequency noise. The red area on the right is a collection of high grayscale values needed to obtain the fluorescence intensity signal. If a specific algorithm finds a global threshold between the noise and signal regions, the noise signal and the fluorescence intensity signal can be well separated.

The adaptive global threshold selection method is proposed for computational complexity problems and poor results of existing threshold selection for binarization. Specifically, the histogram of pixel statistics for the whole image is first calculated and noted as:

$$h(i)_{i=0}^{i=255}$$

Where $i(0 \leq i \leq 255)$ is the gray level, i.e., the horizontal coordinate in Fig. 5a, and $h(i)$ is the total number of image pixels with gray level i, i.e., the vertical coordinate in Fig. 5a.

$$\{h(i)/max_{0 \leq i \leq 255}(h(i))\}_{i=0}^{i=255} \tag{1}$$

$$\{\left(\frac{1}{255}, \frac{h(1)}{max_{0 \leq i \leq 255}(h(1))}\right), \ldots, \left(\frac{i}{255}, \frac{h(i)}{max_{0 \leq i \leq 255}(h(i))}\right)\} \tag{2}$$

Then, we calculate the normalized histogram Formula (1). The final two-dimensional point set is obtained as Eq. (2). Next, binary means clustering is performed on the two-dimensional point set of Eq. (2) to initialize the centroids of two-point sets, $point_0$ and $point_1$. The initial centroid of $point_0$ is $\left(\frac{i_0}{255}, \frac{h(i_0)}{max_{0 \leq i \leq 255}(h(i_0))}\right)$. The initial centroid of $point_1$ is $\left(\frac{i_1}{255}, \frac{h(i_1)}{max_{0 \leq i \leq 255}(h(i_1))}\right)$, where $i_0 = \min_{h(i)\neq 0}(i)$ and $i_1 = \max_{h(i)\neq 0}(i)$.

After convergence of the clustering iteration, the part of the curve between the horizontal coordinates of the two clustering centers is selected. The minimum value of the vertical coordinate is obtained on the selected part of the curve to get the value of the horizontal coordinate corresponding to the minimum value of the vertical coordinate on the curve, which is noted as $\chi_{\min}$. Finally, the value of $\chi_{\min}$ * 255 is used as the global threshold, and the image is binarized according to the obtained global threshold value.

As shown in Fig. 5c, when the fluorescence intensity is weak, "small holes" appear in the image after the adaptive binarization process. As shown in the right column of Fig. 5d, the closing (morphology) is used to bridge the "small holes". Finally, the background noise signal is well removed after the adaptive binarization and the closing (morphology) process. An image containing only the signal of the characterized fluorescence intensity is obtained.

3.2. Restoration of the distorted waveform

The robustness of the volume detection can be significantly improved by using the adaptive global threshold binarization algorithm. However, we ultimately want to calculate the integrated area of the two peaks formed by the fluorescence intensity signals of CL and TL on the time series. By calculating the ratio of the integrated area of the two peaks, PA_{CL}/PA_{TL}The value is used to quantify the concentration of the target material. It is known that the fluorescence intensity signal in the time series can be fitted approximately as a double-peaked Gaussian curve. However, when the concentration of the target is too low, the fluorescence intensity signal in TL will produce a distorted waveform, which still affects the accuracy of quantitative detection and fails to generate a standard Gaussian curve due to the increased chance factor weak signal. Therefore, we propose a waveform reconstruction method to fit a Gaussian function to the fluorescence intensity signal in the time domain. In other words, the algorithm will fit a function approximation to the data point set using a Gaussian function, and the Gaussian function is easy and fast in computing the image integral.

In the specific algorithm implementation, the equal periods for the appearance of fluorescence intensity signals of CL and TL are delineated according to the speed of the stepper motor. The fluorescence intensity signal data are recorded as (t_i, x_i) and (t_i, y_i) for the respective periods, where t_i is the time point of the sampling point and x_i and y_i are the fluorescence intensity at the moment of t_i $(i = 1, 2, 3, \ldots)$.

After that, using the a priori assumption information, it is assumed that (t_i, x_i) can be modelled in Eq. (3) with a Gaussian function:

$$x_i = x_{max} \times exp\left[-\frac{(t_i - t_{max})^2}{S}\right] \tag{3}$$

Where the parameters x_{max}, t_{max} and S to be estimated are the peak, the location of the peak, and the half-width information of the Gaussian curve, respectively. Taking the natural logarithm on both sides of Eq. (3) reduces it to Eq. (4), assuming that $ln_{x_i} = z_i$, $ln_{x_{max}} - \frac{t_{max}^2}{s} = b_0$, $\frac{2t_i t_{max}}{s} = b_1$, $\frac{t_i^2}{s} = b_2$:

$$ln_{x_i} = ln_{x_{max}} - \frac{t_{max}^2}{s} + \frac{2t_i t_{max}}{s} - \frac{t_i^2}{s} \tag{4}$$

Then, all data collected in the respective periods are considered, and the formula is expressed in matrix form as Eq. (5), abbreviated as $Z = XB$:

$$\begin{bmatrix} z_1 \\ \vdots \\ z_i \end{bmatrix} = \begin{bmatrix} 1 & \cdots & t_1^2 \\ \vdots & \ddots & \vdots \\ 1 & \cdots & t_i^2 \end{bmatrix} \bullet \begin{bmatrix} b_0 \\ b_1 \\ b_2 \end{bmatrix} \tag{5}$$

Finally, the generalized least-squares solution of the composition matrix B is then solved according to the least-squares principle to find the parameters x_{max}, t_{max}. S to be estimated. Finally, the characteristic parameters of the estimated Gaussian function are obtained.

The final waveform reconstruction results based on the Gaussian function are shown in Figs. 6a, 6b. The results show that the output of the reconstructed waveforms are all standard Gaussian curves, which further improves the stability and sensitivity of quantitative detection and dramatically simplifies the operation of calculating the integrated area of wave peaks.

4. Results and discussion

In the whole IoT system, we adopted various effective designs and algorithms to improve the accuracy and sensitivity of the system from both a software and hardware perspective. First, the clever hardware design enables a single run to generate two sets of raw data, which reduces the error caused by chance factors and improves the system's accuracy. Second, when calculating the fluorescence intensity signals of CL and TL, a more reliable calculation of the critical area of the waveform is used, significantly improving the system's accuracy. Finally, the image adaptive binarization effectively removes the noise signal and waveform reconstruction algorithm and dramatically reduces the data error and sensitivity degradation due to environmental noise.

On the one hand, to determine the accuracy and lower detection limit of this device, and on the other hand, to verify the effectiveness and robustness of the algorithms proposed in Image denoising and waveform reconstruction processing. We prepared 5 standard assay solutions containing MET at 0, 0.1, 1.0, 10.0, 50.0, and 100.0 ng/ml. After that, data acquisition was performed according to the standard workflow shown in Fig. 4.

The purpose of the adequate ablation experiment is to verify the effectiveness of the image denoising processing module and the waveform reconstruction processing module. Fig. 6c-f visualize the correlation between the quantitative assay results of the device and the MET standard solutions under different conditions. Separately, Fig. 6c shows the results of the original data without the denoising process and waveform reconstruction, with $R^2 = 0.8437$. Fig. 6d shows the results of the experimental data with the denoising process but without waveform reconstruction, with $R^2 = 0.9513$. Fig. 6e shows the results of the experimental data with the waveform reconstruction but without the denoising process, with $R^2 = 0.9701$. Fig. 6f shows the final experimental data with denoising and waveform reconstruction, with R^2 as high as 0.9889.

According to the comparison of the ablation experiments, it is seen that our test results have an excellent linear correlation with the standard MET sample concentration. Among them, the image denoising algorithm improves the results by about 12.7%, the waveform reconstruction algorithm improves the results by about 15.0%, and the overall algorithm module achieves a 17.2% improvement in the

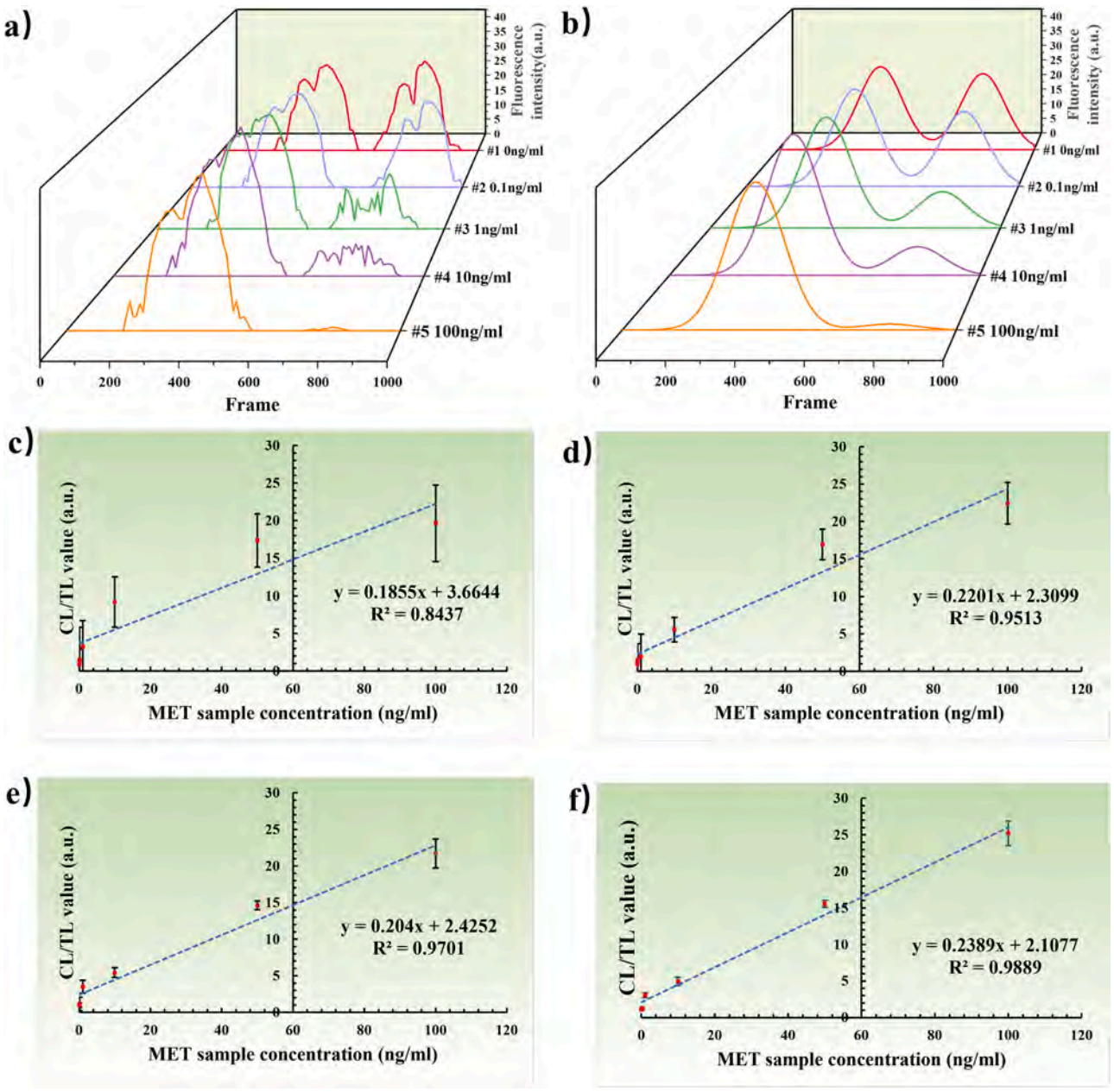

Fig. 6. (a) Schematic diagram of the results after the image adaptive binarization denoising algorithm. It can be seen that the fluorescence intensity signals in the TL region appear significantly different for the 5 different concentrations after filtering out the noise. (b) Schematic diagram of waveform reconstruction results based on Gaussian function. Due to the nature of Gaussian distribution, it is not necessary to use a complex calculation of the integrated area under the curve (which requires finding the peak of the curve and determining the width of the calculation), but to focus directly on only the TL and CL region to estimate the intensity of TL and CL, which will greatly reduce the complexity and improve the applicability of the algorithm. (c) Ablation experiment 1: Fitting results of the original data. (d) Ablation experiment 2: Fitting results with image denoising only. (e) Ablation experiment 3: Fitting results with waveform reconstruction only. (f) Ablation experiment 4: Fitting results with both image denoising and waveform reconstruction.

accuracy and robustness of the final detection results. This result is encouraging and shows that our device is portable in terms of accuracy and robustness. Current MET measurement methods and devices based on different types of probes are compared in Table 1. As the results show, this paper outperforms existing methods and devices in terms of detection time and lower LOD. The designed hardware and enhanced algorithms provide a commercial solution with great potential value for UCNPs in POCT.

In addition, to verify the stability and reproducibility of the equipment. Reproducibility means using the same material, the same experimental equipment, the same operator, and a short time interval under the same conditions. The relative standard deviation between repeated measurements on the same sample is calculated to reveal random variations and errors, affecting the quantitative measurement results. In the experimental evaluation phase, our system was tested 20 times for each sample by applying three different concentrations of standard MET sample, 0.1 ng/ml, 10 ng/ml, and 100 ng/ml, respectively. The statistics are shown in Table 2, where we calculated the mean, Standard Deviation (SD), and Coefficient of Variation (CV%) to verify the whole system's performance. In testing low, medium, and high concentrations of MET standard solutions, the test values for each group fluctuated little around the mean, and the CV% was controlled to some extent. Thus, this indicates that the device has good reproducibility; therefore, the quantitative detection results obtained using the device and algorithm

Table 1
Comparison of the analytical performances of the detection for MET sample with different POCT methods.

Methods	Limit of detection (ng/ml)	Detection range (ng/ml)	Detection time (min)
HPLC [35]	1.7	10–1000	A few seconds
HPLC [36]	30	100–1500	25
GC-MS [37]	150	200–10000	–
GC-MS [38]	0.09	0.09–0.81	12.7
LC-MS [39]	0.2	4–20	20
CE [40]	2	2–500	20
CE [41]	0.5	0.5–50000	15
Quantum dot-based [42]	6	–	1–3
Quantum dot-based [43]	1.8	6.7–400	–
SPR [44]	0.44	–	3
UCNP-LFAs [24]	10	10–250	15
UCNP-LFAs (This work)	0.1	0.1–100	≈ 0.33

Table 2
Statistic results of the stability of the proposed system.

Standard MET concentration (ng/ml)	Test strips #1 Low concentration 0.1	Test strips #2 Mid concentration 10	Test strips #3 High concentration 100
Number of tests	20	20	20
Average (ng/ml)	0.11	10.51	100.73
SD	0.01	0.81	1.11
CV%	8.54	7.72	1.10

developed in this study are stable.

5. Conclusions

In this study, we developed a portable upconversion fluorescence quantification system suitable for roadside detection of drugs. Thanks to an ingenious hardware design, effective fluorescence extraction algorithm, and waveform reconstruction, the system can quickly and automatically denoise and analyze the data and calculate the substance concentration of a small molecule target. We verify the robustness and accuracy through extensive experiments. Usually, the attention of MET in the solution to be tested is 0.2 ng/ml in actual field tests; the system designed in this paper can detect LOD of 0.1 ng/ml within 20 s. Moreover, the test results of MET standard solutions have an excellent linear correlation with the standard value, showing its rapidity and sensitivity. It is worth stating that the hardware and algorithms involved in our proposed IoT system are universally versatile and applicable to all UCNPs-based quantitative assays for small molecule targets. Thus, the commercial device and system architecture we demonstrate here has the advantages of portability, low-cost manufacturing, rapidity, accuracy, and robustness. It provides a solution with great potential value for UCNPs for POCT. It can also be applied to in vitro diagnostics, environmental testing, food analysis, and national security.

Declaration of Competing Interest

The authors declare that they have no known competing financial interests or personal relationships that could have appeared to influence the work reported in this paper.

Acknowledgements

The authors thank the financial support from Shenzhen Science and Technology Program (KQTD20170809110344233) and Shenzhen Bay Laboratory (SZBL201906281005).

References

[1] K. Wang, W. Qin, Y. Hou, K. Xiao, W. Yan, The application of lateral flow immunoassay in point of care testing: a review, Nano Biomed. Eng. 8 (2016) 172–183.
[2] P. Wang, L.J. Kricka, Current and emerging trends in point-of-care technology and strategies for clinical validation and implementation, Clin. Chem. 64 (2018) 1439–1452.
[3] X. Sun, B. Li, C. Tian, F. Yu, N. Zhou, Y. Zhan, L. Chen, Rotational paper-based electrochemiluminescence immunodevices for sensitive and multiplexed detection of cancer biomarkers, Anal. Chim. Acta 1007 (2018) 33–39.
[4] L. Syedmoradi, M. Daneshpour, M. Alvandipour, F.A. Gomez, H. Hajghassem, K. Omidfar, Point of care testing: the impact of nanotechnology, Biosens. Bioelectron. 87 (2017) 373–387.
[5] W. Gao, M. Saqib, L. Qi, W. Zhang, G. Xu, Recent advances in electrochemiluminescence devices for point-of-care testing, Curr. Opin. Electrochem. 3 (2017) 4–10.
[6] Z. Liang, X. Wang, W. Zhu, P. Zhang, Y. Yang, C. Sun, J. Zhang, X. Wang, Z. Xu, Y. Zhao, et al., Upconversion nanocrystals mediated lateral-flow nanoplatform for in vitro detection, ACS Appl. Mater. \ Interfaces 9 (2017) 3497–3504.
[7] Q. Ju, M.O. Noor, U.J. Krull, based biodetection using luminescent nanoparticles, Analyst 141 (2016) 2838–2860.
[8] K. Mahato, A. Srivastava, P. Chandra, Paper based diagnostics for personalized health care: emerging technologies and commercial aspects, Biosens. Bioelectron. 96 (2017) 246–259.
[9] S.C.B. Gopinath, T. Lakshmipriya, Y. Chen, W.-M. Phang, U. Hashim, Aptamer-based 'point-of-care testing, Biotechnol. Adv. 34 (2016) 198–208.
[10] O. Mudanyali, S. Dimitrov, U. Sikora, S. Padmanabhan, I. Navruz, A. Ozcan, Integrated rapid-diagnostic-test reader platform on a cellphone, Lab a Chip 12 (2012) 2678–2686.
[11] D. Quesada-González, A. Merkoçi, Nanoparticle-based lateral flow biosensors, Biosens. Bioelectron. 73 (2015) 47–63.
[12] E. Eltzov, S. Guttel, A. Low Yuen Kei, P.D. Sinawang, R.E. Ionescu, R.S. Marks, Lateral flow immunoassays–from paper strip to smartphone technology, Electroanalysis 27 (2015) 2116–2130.
[13] S. Shikha, T. Salafi, J. Cheng, Y. Zhang, Versatile design and synthesis of nano-barcodes, Chem. Soc. Rev. 46 (2017) 7054–7093.
[14] F. Wang, R. Deng, J. Wang, Q. Wang, Y. Han, H. Zhu, X. Chen, X. Liu, Tuning upconversion through energy migration in core–shell nanoparticles, Nat. Mater. 10 (2011) 968–973.
[15] W. Kong, T. Sun, B. Chen, X. Chen, F. Ai, X. Zhu, M. Li, W. Zhang, G. Zhu, F. Wang, A general strategy for ligand exchange on upconversion nanoparticles, Inorg. Chem. 56 (2017) 872–877.
[16] Z. Zhang, S. Shikha, J. Liu, J. Zhang, Q. Mei, Y. Zhang, Upconversion nanoprobes: recent advances in sensing applications, Anal. Chem. 91 (2018) 548–568.
[17] C. Wang, X. Li, F. Zhang, Bioapplications and biotechnologies of upconversion nanoparticle-based nanosensors, Analyst 141 (2016) 3601–3620.
[18] X. Zhu, Q. Su, W. Feng, F. Li, Anti-Stokes shift luminescent materials for bio-applications, Chem. Soc. Rev. 46 (2017) 1025–1039.
[19] B. Gu, Q. Zhang, Recent advances on functionalized upconversion nanoparticles for detection of small molecules and ions in biosystems, Adv. Sci. 5 (2018), 1700609.
[20] A. Gulzar, J. Xu, P. Yang, F. He, L. Xu, Upconversion processes: versatile biological applications and biosafety, Nanoscale 9 (2017) 12248–12282.
[21] Q. Su, W. Feng, D. Yang, F. Li, Resonance energy transfer in upconversion nanoplatforms for selective biodetection, Acc. Chem. Res. 50 (2017) 32–40.
[22] J. Guo, S. Chen, J. Guo, X. Ma, Nanomaterial labels in lateral flow immunoassays for point-of-care-testing, J. Mater. Sci. Technol. 60 (2021) 90–104.
[23] S.R. Ahmed, R. Chand, S. Kumar, N. Mittal, S. Srinivasan, A.R. Rajabzadeh, Recent biosensing advances in the rapid detection of illicit drugs, Trends Anal. Chem. 131 (2020), 116006.
[24] Q. Hu, Q. Wei, P. Zhang, S. Li, L. Xue, R. Yang, C. Wang, L. Zhou, An up-converting phosphor technology-based lateral flow assay for point-of-collection detection of morphine and methamphetamine in saliva, Analyst 143 (2018) 4646–4654.
[25] Q. Mei, H. Jing, Y. Li, W. Yisibashaer, J. Chen, B.N. Li, Y. Zhang, Smartphone based visual and quantitative assays on upconversional paper sensor, Biosens. Bioelectron. 75 (2016) 427–432.
[26] X. Zhao, Y. Fu, C. Ren, J. Guo, Y. Kang, Quantitative detection of morphine based on an up-conversion luminescent system, Analyst 146 (2021) 989–996.
[27] R. Chand, N. Mittal, S. Srinivasan, A.R. Rajabzadeh, Upconverting nanoparticle clustering based rapid quantitative detection of tetrahydrocannabinol (THC) on lateral-flow immunoassay, Analyst 146 (2021) 574–580.
[28] Y. Jung, Y. Heo, J.J. Lee, A. Deering, E. Bae, Smartphone-based lateral flow imaging system for detection of food-borne bacteria E. coli O157: H7, J. Microbiol Methods 168 (2020), 105800.
[29] W. Xiao, C. Huang, F. Xu, J. Yan, H. Bian, Q. Fu, K. Xie, L. Wang, Y. Tang, A simple and compact smartphone-based device for the quantitative readout of colloidal gold lateral flow immunoassay strips, Sens. Actuators B Chem. 266 (2018) 63–70.
[30] B. Jin, Y. Yang, R. He, Y. il Park, A. Lee, D. Bai, F. Li, T.J. Lu, F. Xu, M. Lin, Lateral flow aptamer assay integrated smartphone-based portable device for simultaneous detection of multiple targets using upconversion nanoparticles, Sens. Actuators B Chem. 276 (2018) 48–56.
[31] H.J. Min, H.A. Mina, A.J. Deering, E. Bae, Development of a smartphone-based lateral-flow imaging system using machine-learning classifiers for detection of Salmonella spp, J. Microbiol Methods 188 (2021).

[32] H. Kim, Y. Jung, I.J. Doh, R.A. Lozano-Mahecha, B. Applegate, E. Bae, Smartphone-based low light detection for bioluminescence application, Sci. Rep. (2017) 1–11, 2017 7:1. 7.
[33] Labrox, Upconverting Nanoparticle System, (2008).
[34] T. Soukka, K. Kuningas, T. Rantanen, V. Haaslahti, T. Lövgren, Photochemical characterization of up-converting inorganic lanthanide phosphors as potential labels, J. Fluor. 15 (2005) 513–528.
[35] R. Wang, X. Qi, L. Zhao, S. Liu, S. Gao, X. Ma, Y. Deng, Ionic-liquid-based dispersive liquid–liquid microextraction coupled with high-performance liquid chromatography for the forensic determination of methamphetamine in human urine, J. Sep. Sci. 39 (2016) 2444–2450.
[36] A. Taghvimi, H. Hamishehkar, M. Ebrahimi, The application of magnetic nano graphene oxide in determination of methamphetamine by high performance liquid chromatography of urine samples, J. Iran. Chem. Soc. 13 (2016) 1471–1480.
[37] S. Peng, G. Xin, J. Wang, Y. Wang, J. Meng, GC-MS qualitative analysis of methamphetamine, MDMA and ketamine in urine under full scan mode, Forensic Science and Technology 45 (1) (2020) 24.
[38] M.K. Woźniak, M. Wiergowski, J. Aszyk, J. Kubica Paweł and Namieśnik, M. Biziuk, Application of gas chromatography–tandem mass spectrometry for the determination of amphetamine-type stimulants in blood and urine, J. Pharm. Biomed. Anal. 148 (2018) 58–64.
[39] M. Zhao, Z. Wang, S. Liu, W. Zhang, L.I. Hong, Simultaneous determination of three drugs in saliva by UPLC-MS/MS, Chin. J. Forensic Med. 33 (2018) 65–67.
[40] M. Rezazadeh, Y. Yamini, S. Seidi, Application of a new nanocarbonaceous sorbent in electromembrane surrounded solid phase microextraction for analysis of amphetamine and methamphetamine in human urine and whole blood, J. Chromatogr. A 1396 (2015) 1–6.
[41] P. Saar-Reismaa, E. Erme, M. Vaher, M. Kulp, M. Kaljurand, J. Mazina-Šinkar, In situ determination of illegal drugs in oral fluid by portable capillary electrophoresis with deep UV excited fluorescence detection, Anal. Chem. 90 (2018) 6253–6258.
[42] M. Masteri-Farahani, N. Mosleh, Modified CdS quantum dots as selective turn-on fluorescent nanosensor for detection and determination of methamphetamine, J. Mater. Sci.: Mater. Electron. 30 (2019) 21170–21176.
[43] J. Hassanzadeh, A. Khataee, R. Lotfi, Sensitive fluorescence and chemiluminescence procedures for methamphetamine detection based on CdS quantum dots, Microchem. J. 132 (2017) 371–377.
[44] J. Wang, W. Yao, F. Meng, P. Wang, Y. Wu, B. Wang, A surface plasmon resonance immunoassay for the rapid analysis of methamphetamine in forensic oral fluid, J. Clin. Lab Anal. 33 (2019), e22993.
[45] R.J. Martino, S. Shiau, K.D. Krause, P.N. Halkitis, Event-level patterns of methamphetamine and poly-drug use among millennial sexual minority men: the P18 Cohort Study, Addict. Behav. 117 (2021), 106831.
[46] S. Darke, J. Duflou, S. Kaye, Prevalence and nature of cardiovascular disease in methamphetamine-related death: a national study, Drug Alcohol Depend. 179 (2017) 174–179.
[47] R. Ahrnsbrak, J. Bose, S.L. Hedden, R.N. Lipari, E. Park-Lee, Substance Abuse and Mental Health Services Administration. Key substance use and mental health indicators in the United States: results from the 2016 National Survey on Drug Use and Health, (2019).
[48] K. Dombrowski, D. Crawford, B. Khan, K. Tyler, Current rural drug use in the US Midwest, J. Drug Abus. 2 (2016).
[49] X. Ma, X. Wang, K. Hahn, S. Sánchez, Motion control of urea-powered biocompatible hollow microcapsules, ACS Nano 10 (2016) 3597–3605.
[50] Y. You, D. Xu, X. Pan, X. Ma, Self-propelled enzymatic nanomotors for enhancing synergetic photodynamic and starvation therapy by self-accelerated cascade reactions, Appl. Mater. Today 16 (2019) 508–517.
[51] R. Han, H. Yi, J. Shi, Z. Liu, H. Wang, Y. Hou, Y. Wang, pH-Responsive drug release and NIR-triggered singlet oxygen generation based on a multifunctional core–shell–shell structure, Phys. Chem. Chem. Phys. 18 (2016) 25497–25503.

Wei Wang received is currently pursuing the degree in biomedical equipment, chemical sensors, and computer vision with the School of Information and Communication Engineering, University of Electronic Science and Technology of China.

Zihan Ye received his master's degree from the Institute of Polymer Chemistry, Nankai University, Tianjin, China, in 2018. He is now a Ph.D. candidate at the School of Materials Science and Engineering, Harbin Institute of Technology (ShenZhen), China. His research activities involve the synthesis of micro-nanomotors and movement control with applications for biomedicine.

Xing Ma received his B.S. in Welding Technology and Engineering from Harbin Institute of Technology in 2009. And then he obtained his Ph.D. degree in Materials Science and Engineering from Nanyang Technological University in 2013. He used to work as Alexander von Humboldt research fellow at Max-Planck Institute for Intelligent Systems (MPI-IS) at Stuttgart, Germany, from 2014 to 2016. His research interest focuses on enzyme powered mesoporous silica micro/nanomotors for active drug delivery, and nanodevices for biosensing. He has been awarded the China Thousand Talents Plan for Young Scholars Award (2016) and Shenzhen Peacock Talent Program of Category B (2017). In 2016, Dr. Xing Ma was awarded the Gunter Petzow Prize from MPI-IS for his achievement in enzyme powered micro/nanomotors. He has been working as a professor in the School of Materials Science and Engineering at Harbin Institute of Technology (Shenzhen) since 2016.

Jinhong Guo received the bachelor's degree in electronic engineering from the University of Electronic Science and Technology of China, Chengdu, China in 2010 and PhD degree in biomedical engineering from the Nanyang Technological University in 2014. Currently, he is a full professor in the School of Information and Communication Engineering, University of Electronic Science and Technology of China and Chengdu University of Traditional Medicine, Chengdu, China. After his doctoral studies, he was a postdoctoral fellow in the Pillar of Engineering Design at MIT-SUTD Singapore from 2014 to 2015. He then worked as a Visiting Professor in the School of Mechanical Engineering at University of Michigan, Ann Arbor from January 2016 to July 2016. His current research focuses on Electrochemical Sensor and lab-on-a-chip devices for Point of Care Test toward clinical use. He is a recipient of the China Sichuan Thousand Talents Plan for Scholars Award (2015) and Chengdu Expert in Science and Technology Award (2015). He has published over 100 publication in SCI journal such as IEEE TII, TBME, TBioCAS, Analytical Chemistry, Biosensor and Bioelectronics etc.